Two dimensional hard x-ray nanofocusing with crossed multilayer Laue lenses

Hanfei Yan,[1,3] Volker Rose,[2] Deming Shu,[2] Enju Lima,[3] Hyon Chol Kang,[4] Ray Conley,[2,3] Chian Liu,[2] Nima Jahedi,[2] Albert T. Macrander,[2] G. Brian Stephenson,[1] Martin Holt,[1] Yong S. Chu,[3] Ming Lu,[5] and Jörg Maser[1,2*]

[1]*Center for Nanoscale Materials, Argonne National Laboratory, Argonne, Illinois 60439, USA*
[2]*Advanced Photon Source, Argonne National Laboratory, Argonne, Illinois 60439, USA*
[3]*National Synchrotron Light Source II, Brookhaven National Laboratory, Upton, New York 11973, USA*
[4]*Department of Advanced Materials Engineering and BK21 Education Center of Mould Technology for Advanced Materials and Parts, Chosun University, Gwangju 501-759, South Korea*
[5]*Center for Functional Nanomaterials, Brookhaven National Laboratory, Upton, New York 11973, USA*
**maser@anl.gov*

Abstract: Hard x-ray microscopy with nanometer resolution will open frontiers in the study of materials and devices, environmental sciences, and life sciences by utilizing the unique characterization capabilities of x-rays. Here we report two-dimensional nanofocusing by multilayer Laue lenses (MLLs), a type of diffractive optics that is in principle capable of focusing x-rays to 1 nm. We demonstrate focusing to a 25 × 27 nm^2 FWHM spot with an efficiency of 2% at a photon energy of 12 keV, and to a 25 × 40 nm^2 FWHM spot with an efficiency of 17% at a photon energy of 19.5 keV.

OCIS codes: (050.1970) Diffractive optics; (180.7460) X-ray microscopy.

References and links

1. H. Mimura, H. Yumoto, S. Matsuyama, Y. Sano, K. Yamamura, Y. Mori, M. Yabashi, Y. Nishino, K. Tamasaku, T. Ishikawa, and K. Yamauchi, "Efficient focusing of hard x rays to 25 nm by a total reflection mirror," Appl. Phys. Lett. **90**(5), 051903 (2007).
2. G.-C. Yin, Y.-F. Song, M.-T. Tang, F.-R. Chen, K. S. Liang, F. W. Duewer, M. Feser, W. Yun, and H.-P. D. Shieh, "30 nm resolution x-ray imaging at 8 keV using third order diffraction of a zone plate lens objective in a transmission microscope," Appl. Phys. Lett. **89**(22), 221122 (2006).
3. C. G. Schroer, O. Kurapova, J. Patommel, P. Boye, J. Feldkamp, B. Lengeler, M. Burghammer, C. Riekel, L. Vincze, A. van der Hart, and M. Kuchler, "Hard X-ray nanoprobe based on refractive x-ray lenses," Appl. Phys. Lett. **87**(12), 124103 (2005).
4. W. Chao, B. D. Harteneck, J. A. Liddle, E. H. Anderson, and D. T. Attwood, "Soft X-ray microscopy at a spatial resolution better than 15 nm," Nature **435**(7046), 1210–1213 (2005).
5. J. Vila-Comamala, K. Jefimovs, J. Raabe, T. Pilvi, R. H. Fink, M. Senoner, A. Maaßdorf, M. Ritala, and C. David, "Advanced thin film technology for ultrahigh resolution X-ray microscopy," Ultramicroscopy **109**(11), 1360–1364 (2009).
6. H. Mimura, S. Handa, T. Kimura, H. Yumoto, D. Yamakawa, H. Yokoyama, S. Matsuyama, K. Inagaki, K. Yamamura, Y. Sano, K. Tamasaku, Y. Nishino, M. Yabashi, T. Ishikawa, and K. Yamauchi, "Breaking the 10 nm barrier in hard-X-ray focusing," Nat. Phys. **6**(2), 122–125 (2010).
7. S. Matsuyama, H. Mimura, H. Yumoto, Y. Sano, K. Yamamura, M. Yabashi, Y. Nishino, K. Tamasaku, T. Ishikawa, and K. Yamauchi, "Development of scanning X-ray fluorescence microscope with spatial resolution of 30 nm using Kirkpatrick-Baez mirror optics," Rev. Sci. Instrum. **77**(10), 103102 (2006).
8. H. C. Kang, J. Maser, G. B. Stephenson, C. Liu, R. Conley, A. T. Macrander, and S. Vogt, "Nanometer linear focusing of hard X rays by a multilayer Laue lens," Phys. Rev. Lett. **96**(12), 127401 (2006).
9. A. T. Macrander, H. Yan, H. C. Kang, J. Maser, C. Liu, R. Conley, and G. B. Stephenson, "Nanofocusing of hard X-rays with multilayer laue lenses," in *Hand Book of Optics*(McGraw-Hill Professional, 2009).
10. H. F. Yan, J. Maser, A. Macrander, Q. Shen, S. Vogt, G. B. Stephenson, and H. C. Kang, "Takagi-Taupin description of x-ray dynamical diffraction from diffractive optics with large numerical aperture," Phys. Rev. B **76**(11), 115438 (2007).
11. H. F. Yan, "X-ray dynamical diffraction from multilayer Laue lenses with rough interfaces," Phys. Rev. B **79**(16), 165410 (2009).

#145575 - $15.00 USD Received 7 Apr 2011; revised 19 May 2011; accepted 22 May 2011; published 21 Jul 2011

12. H. C. Kang, G. B. Stephenson, C. Liu, R. Conley, R. Khachatryan, M. Wieczorek, A. T. Macrander, H. Yan, J. Maser, J. Hiller, and R. Koritala, "Sectioning of multilayers to make a multilayer Laue lens," Rev. Sci. Instrum. **78**(4), 046103 (2007).
13. H. C. Kang, H. F. Yan, R. P. Winarski, M. V. Holt, J. Maser, C. A. Liu, R. Conley, S. Vogt, A. T. Macrander, and G. B. Stephenson, "Focusing of hard x-rays to 16 nanometers with a multilayer Laue lens," Appl. Phys. Lett. **92**(22), 221114 (2008).
14. J. Maser, G. B. Stephenson, S. Vogt, Y. Wenbing, A. Macrander, H. C. Kang, L. Chian, and R. Conley, "Multilayer Laue lenses as high-resolution x-ray optics," Proc. SPIE - Int. Soc. Opt. Eng. **5539**, 185–194 (2004).
15. H. Yan, J. Maser, H. C. Kang, A. Macrander, and B. Stephenson, "A theoretical study of two-dimensional point focusing by two multilayer Laue lenses," Proc. SPIE - Int. Soc. Opt. Eng. **7077**, 70770Q–70778 (2008).
16. H. M. Quiney, A. G. Peele, Z. Cai, D. Paterson, and K. A. Nugent, "Diffractive imaging of highly focused X-ray fields," Nat. Phys. **2**(2), 101–104 (2006).
17. D. Shu, H. Yan, and J. Maser, "Mechanical design of a multi-dimensional alignment system for an MLL system with nanometerscale 2-D focusing," in *Proceedings of SRI-2008*(to be published in Nucl. Instrum. Methods A, Saskatoon, Canada, 2008).
18. D. Shu, H. Yan, and J. M. Maser, "Multidimensional alignment apparatus for hard x-ray focusing with two multilayer Laue lenses," US Patent No. 7597475 (6 October 2009).
19. http://www.xradia.com.
20. D. M. Bates, and D. G. Watts, *Nonlinear Regression Analysis and Its Applications* (John Wiley & Sons, Inc., 1988).
21. B. M. Weckhuysen, "Chemical imaging of spatial heterogeneities in catalytic solids at different length and time scales," Angew. Chem. Int. Ed. Engl. **48**(27), 4910–4943 (2009).
22. T. Paunesku, S. Vogt, J. Maser, B. Lai, and G. Woloschak, "X-ray fluorescence microprobe imaging in biology and medicine," J. Cell. Biochem. **99**(6), 1489–1502 (2006).
23. R. Conley, C. Liu, J. Qian, C. M. Kewish, A. T. Macrander, H. Yan, H. C. Kang, J. Maser, and G. B. Stephenson, "Wedged multilayer Laue lens," Rev. Sci. Instrum. **79**(5), 053104 (2008).

1. Introduction

X-ray microscopy is complementary to other types of microscopy. Because of their weak interaction with matter, x-rays can penetrate into materials, allowing the study of buried interfaces and internal sample structures without invasive sample preparation. X-rays are insensitive to electric and magnetic fields and allow measurements in ambient environment or gases. This makes them uniquely suitable for in situ studies. They further provide a very high elemental sensitivity to trace elements, as well as a high accuracy in quantifying elemental and structural properties of matter. It has been difficult to date to achieve efficient focusing of hard x-rays to spots of 50 nm or below. To improve the spatial resolution significant effort has been invested in the last decade into advancing the state-of-the-art of x-ray optics. Optics such as mirrors [1], zone plates [2] and refractive lenses [3] are now capable of focusing hard x-rays to well below 100 nm. Fresnel zone plates have shown the highest two-dimensional (2D) spatial resolution of below 15 × 15 nm^2 in the soft x-ray range [4, 5] and refractive optics have achieved ~50 × 50 nm^2 in 2D [3]. Development of reflective optics has shown remarkable progress, resulting recently in a one-dimensional line focus of 7 nm obtained by a multilayer Kirkpatrick–Baez (K-B) mirror at a one kilometer long beamline [6]. 2D nanofocusing of 30 × 50 nm^2 by K-B mirrors has also been reported [7].

We have pursued the development of multilayer Laue lenses (MLLs) as a path to focusing of x-rays to a few nanometers [8, 9]. MLLs are diffractive optics that can focus x-rays to 1 nm at very high focusing efficiency [10] even when the MLL is imperfect [11]. They are used in transmission (Laue) geometry and are therefore less sensitive to angular misalignment and surface figure errors than reflective optics. MLLs are fabricated by sputter deposition followed by sectioning and thinning [12]. This approach provides high aspect ratios of 10^3:1 to 10^4:1 required for efficient nanometer focusing. Using a single MLL, we have demonstrated focusing of hard x-rays with into a 16 nm wide line with an efficiency of 31% [13]. We report here nanoscale 2D imaging with 25 × 27 nm^2 resolution at a photon energy of 12 keV, and with 25 × 40 nm^2 resolution at 19.5 keV obtained by using two MLLs placed in a crossed geometry [14, 15].

#145575 - $15.00 USD Received 7 Apr 2011; revised 19 May 2011; accepted 22 May 2011; published 21 Jul 2011

2. Focusing property of MLL optics

It is important to understand the complex wavefield after a pair of MLLs, in particular the intensity distribution on their common focal plane and in the far-field, where it can be captured by area detectors. Like other diffractive optics, an MLL can diffract incident x-rays into multiple diffraction orders and correspondingly into different foci for these orders. The diffracted wavefield then consists of cylindrical waves converging to (or diverging from) different foci, with the intensity in each order depending on the details of the diffraction geometry (see Fig. 1(a)). Two MLLs assembled in a crossed geometry have a wavefield that consist of a superposition of the wavefronts. If we denote the cylindrical waves emitting from the first MLL as 0, ± 1, ± 2, …, corresponding to different diffraction orders, waves diffracted by two consecutive MLLs can be denoted by indices (i,j), where the i is the index for the horizontally focusing MLL and j is the index for the vertically focusing MLL. So, for example, the (0, 0) wave is for the direct transmitted beam, and (–1, –1) is for the wave diffracted into a two-dimensional focus by diffraction by two consecutive MLL sections, (–1, 0) is for the wave forming a vertically focused line, and (0, –1) is for the wave forming a horizontallyfocused line. A detailed theoretical discussion about the wave propagation through two crossed MLLs can be found elsewhere [15]. Here we present new simulation results.

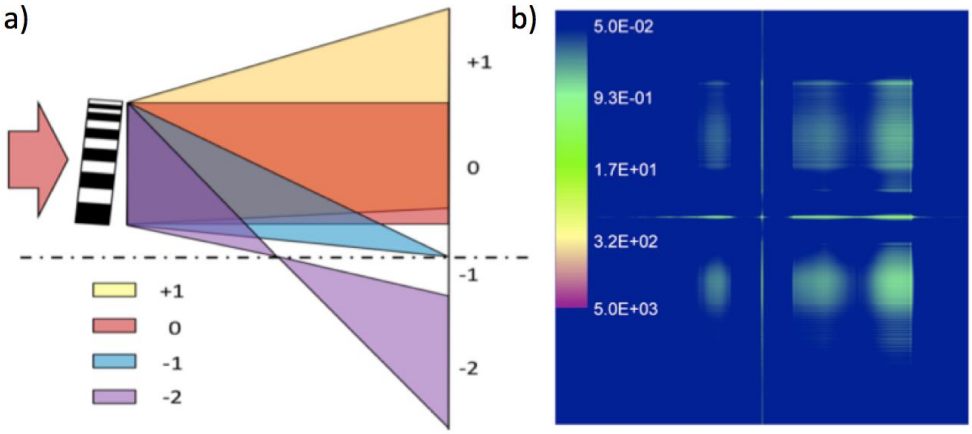

Fig. 1. (a) A schematic drawing of the wavefronts after one MLL. Only first few orders are shown. (b) The simulated intensity distribution on the common focal plane of a pair of crossed MLLs. The dimensions of the image are 45 x 45 μm^2. The point focus is located at the center.

The MLLs under consideration correspond to the ones used at a photon energy of 19.5 KeV, as described in the following section. In Fig. 1(b) we depict the intensity distribution in the focal plane of the first order for both MLLs. The intense point at the center of Fig. 1 is the 2D focus formed by a pair of MLLs, waves (–1, –1). There are crossed lines dividing the diffraction patterns into four quadrants, which correspond to line foci from two cylindrical waves diffracted by one of the MLLs but transmitting through the other MLL (waves (–1,0) and (0,-1)). It should be noted that the crossed lines also contain waves with other combinations, such as (–1, +1), (+1, –1), (–1, –2), (–1, –3), (–2, –1), (–3, –1)… etc. The broken spacing separating the line foci from the point focus is due to the fact that partial MLLs are used, and have no diffracting structure for the lower spatial frequencies. Diffracted waves corresponding to unfocused or diverging waves are found in the four quadrants. The upper right quadrant corresponds mostly to undiffracted beam (0, 0), with the dark band in the

#145575 - $15.00 USD Received 7 Apr 2011; revised 19 May 2011; accepted 22 May 2011; published 21 Jul 2011

vertical direction representing the fraction of the incident beam diffracted into the horizontal focusing first order, i.e. extinction in the part of the MLL where the Bragg condition is satisfied. The effect is not apparent in the other direction because the vertical MLL diffracts much less dynamically. The lower right and upper left quadrants corresponds mostly to vertically diverging and horizontally diverging cylinder waves, with the dark lines corresponding to extinction in the 0th order from one MLL. The lower left quadrant corresponds to the diverging spherical wavefront after diffraction by both MLLs. Because the Bragg condition is satisfied for the focusing orders, the intensity for the positive (diverging) order is very low. In general, an OSA is placed around the focal spot to block all diffraction orders other than the focused beam (wave (−1, −1). For the out-of plane geometry we choose, this is not required if, as in our case, an isolated small object is chosen as the test pattern.

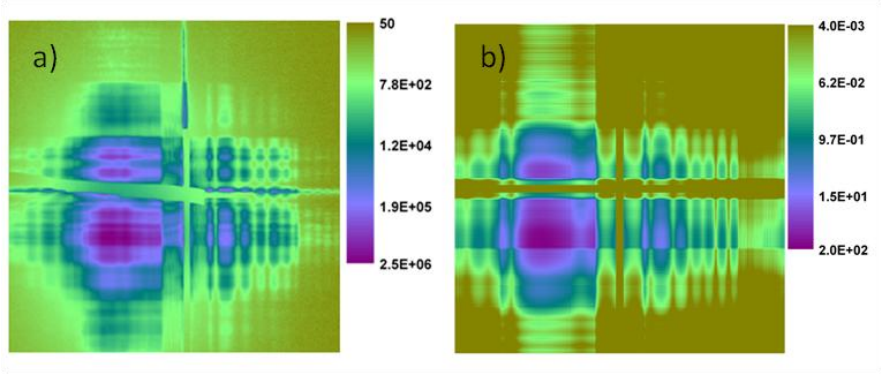

Fig. 2. a) The measured far field diffraction pattern from a pair of crossed MLLs and b) the corresponding simulation. A cross beamstop blocking the direct beam and two line foci is used in both graphs.

For a comparison with the experiment, we show both the measured (Fig. 2(a)) and the simulated (Fig. 2(b)) far field diffraction patterns. A cross-shaped beamstop is utilized to block the direct beam and two line foci. The far field image depicts complex patterns resulting from interference between different diffraction orders. The intensity distribution in the lower left quadrant corresponds to the wave (−1, −1), i.e. corresponds to the point focus shown in Fig. 1, while these in other quadrants from other diffraction orders. The asymmetry of the pattern arises from the tilted geometry, i.e., the negative first order for focusing is enhanced while diverging orders are suppressed. One may notice that there are additional features in the measured image as compared to the simulated one. They may be caused by imperfection of the lens, non plane-wave illumination or misalignment. In order to do a quantitative analysis, a wavefield reconstruction by phase retrieval techniques will be necessary [16].

3. Experiment and results

For two-dimensional focusing, the wave (−1,-1), as discussed above, is used. To achieve a two-dimensional focus, we mounted two MLLs with different focal lengths in a prototype MLL microscope and aligned them to have the same focal plane. Figure 3(a) shows the required degrees for alignment for the two MLLs. The MLL used for horizontal focusing (hMLL) is the same at two different energies. It consists of 1588 alternating WSi_2 and Si layers with layer thicknesses ranging from 25 nm to 5 nm and a total deposition thickness of 13.4 μm. This structure corresponds to 40% of the acceptance of an equivalent full structure, with a diffraction-limited resolution of 12.5 nm. It has a focal length of 1.6 mm at 12 keV (wavelength $\lambda = 0.103$ nm) and 2.6 mm at 19.5 keV (wavelength $\lambda = 0.064$ nm). The MLL used for vertical focusing (vMLL) at 12 keV consists of 2579 alternating WSi_2 and Si layers with layer thicknesses ranging from 25 nm to 5 nm and a total deposition thickness of 21.5

#145575 - $15.00 USD Received 7 Apr 2011; revised 19 May 2011; accepted 22 May 2011; published 21 Jul 2011

μm. The structure has an acceptance of 40% of the full structure as well, and a diffraction limited resolution of 12.5 nm. Its focal length at 12 keV is 2.6 mm, providing a gap of 1 mm between hMLL and vMLL to allow alignment in angle and position, and yielding a working distance of 1.6 mm. For the vertical focusing at a photon energy of 19.5 keV, we used an MLL with a total of 728 alternating WSi_2 and Si layers with layer thicknesses ranging from 30 nm to 10 nm and a total deposition thickness of 12.4 μm. The structure has an acceptance of 40% of the full structure, and a diffraction limited resolution of 25 nm. Its focal length at 19.5 keV is 4.7 mm.

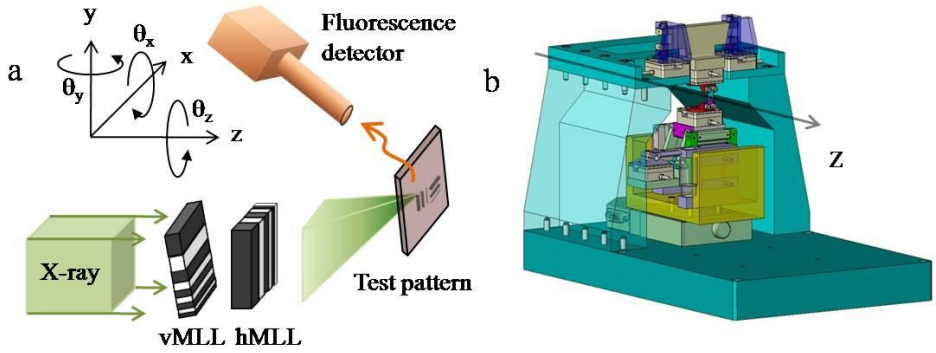

Fig. 3. a) Degrees of freedom for motion required for aligning two crossed MLLs for 2D focusing. b) 3D model of the MLL positioner. The top and bottom parts provide the degrees of freedom needed to align two MLLs for 2D focusing. The incident radiation is along the z axis. For clarity, the sample stage is not shown.

In order to obtain a point focus at the same focal plane, the two lenses have to be fully aligned, i.e., they have to individually meet the Bragg condition and have to be spaced along the optical axis by the difference in focal length. We have developed a MLL-based microscope that is capable of providing the degrees of freedom required for alignment of two MLLs with respect to the incoming x-rays at the required high mechanical stability [17, 18]. Specimen positioning is achieved with commercial flexure-based sample scanners. The MLL positioner is depicted in Fig. 3(b). It consists of two sets of manipulators. The lower set of manipulators, used for the upstream vMLL, has a unique nested flexural bearing structure. It consists of a U-shaped base frame for y and θ_x motions, and a 4-bar flexural bearing structure for x and θ_z motions. The stage is attached to a base linear motor for z motion. The upper set of manipulators, used for the downstream hMLL, consists of a carriage driven by two linear stages for z and θy motions, and a linear stage attached to the carriage for x motion. The flexure design ensures a high stiffness to achieve the long-term mechanical stability required for nanometer resolution. A vibration test shows that the apparatus does not amplify the vibration from the mounting base [17]. The eight degrees of freedom allow the alignment of both MLLs to the correct Bragg angle, focusing of each MLL into the same focal plane, and lateral alignment on the center of the incident x-ray beam.

The experiment was conducted at beamline 26-ID at the Advanced Photon Source at Argonne National Laboratory. Photon energies of 12 keV and 19.5 keV, respectively, were chosen using a double crystal monochromator with an angular stability of ~0.2 μrad. Monochromatic beam was apertured by a pair of slits with a size of 15 × 22 μm^2 at 12 keV and 15 × 15 μm^2 at 19.5 keV. As a first step, each MLL was aligned individually. This involves lateral positioning into the incident x-ray beam, and tilting the MLL to the proper Bragg angle. We have measured the individual focusing efficiency of each MLL, as well as the net efficiency. Figure 4 shows the zero order transmission vs. lens position at two different tilting angles; on the Bragg condition (squares) and off the Bragg condition (circles). The difference in transmission for the two curves corresponds to the diffraction extinction, and is

#145575 - $15.00 USD Received 7 Apr 2011; revised 19 May 2011; accepted 22 May 2011; published 21 Jul 2011

approximately equivalent to the focusing efficiency of the lens, since most of the diffracted intensity goes to the primary focusing order [10]. At a photon energy of 12 keV, the measured individual efficiency was 10% and 20% for vMLL and hMLL, respectively. This corresponds to a net efficiency of 2% for the 2D focusing configuration, and a focused flux of $6x10^6$ photons/sec. The focused flux is currently limited by the small acceptance of the optics, which captures 2% of the coherent flux. The relatively low efficiency at 12 keV is due to strong absorption at the low energy as well as a non-optimum section depth of the lens. Theoretically, over 4% 2D efficiency can be achieved. By fabricating an MLL with an acceptance corresponding to the lateral coherence length of 120 micrometers at 12 keV, an additional factor 50 in focused flux could be obtained. At a photon energy of 19.5 keV, the measured net efficiency was 17% (46% for vMLL and 37% for hMLL), which is far beyond what Fresnel zone plates can achieve today at this energy. Currently, zone plates with a diffraction-limited focus of 30 nm can achieve an efficiency of 1 - 2% at photon energy of 10 keV, and less at higher energies [19].

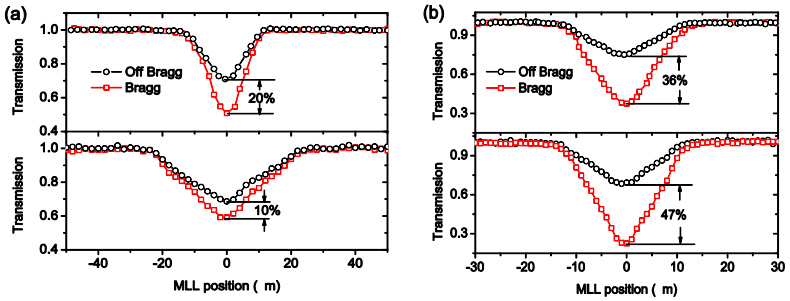

Fig. 4. Transmission curve vs. MLL position at two different angles and at (a) 12 keV and (b) 19.5 keV when the lens is fully illuminated for vMLL (top panel) and hMLL (bottom panel).

After alignment of the MLLs, we positioned a test pattern into the focused beam to quantify the spatial resolution. The object imaged is a gold pattern fabricated by a lift-off lithography method offering various feature sizes from 200 nm down to 50 nm. The thickness of the gold film is about 100 nm. Figure 5(a) is the scanning electron microscope (SEM) image of the grating. The narrowest four lines in both directions have line/space widths of 50 nm. Figure 5(b) and 5(c) are the x-ray scanning images, where the intensity corresponds to the L_β line of Au. As one can see from the fluorescence mapping, gratings are clearly resolved in both directions, indicating a resolution much better than 50 nm.

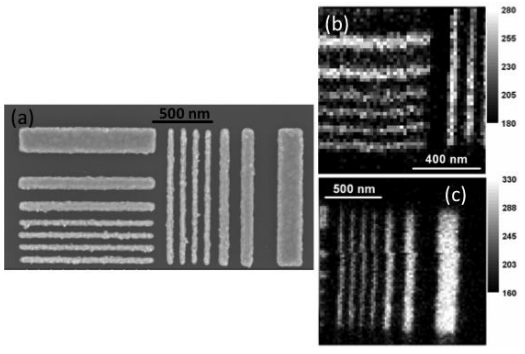

Fig. 5. SEM images of Au gratings (a) and its x-ray scanning images (b) and (c). Exposure time per pixel is 1 second, with a maximum count rate in the gold L_β line of 300 counts/sec. The kink seen in c) is due to the beam dump during the data acquisition. The pixel dimensions in (b) and (c) are 20 × 20 nm^2.

#145575 - $15.00 USD Received 7 Apr 2011; revised 19 May 2011; accepted 22 May 2011; published 21 Jul 2011

In order to quantify the resolution, a line scan across an isolated 50-nm line was fitted by the convolution of the focus profile and a square function of width 50 nm. For simplicity, we assume that the focus profile can be represented by multi-Gaussian peaks. Figure 6(a) and 6(b) show the fitted focus profile and the fitting to the experimental data in each direction based on a non-linear least-square fitting algorithm [20]. Utilizing the full width at half maximum (FWHM) of the focus, we obtain a resolution of 25 nm in horizontal and 27 nm in vertical directions at a photon energy of 12 keV. We also conducted the experiment at 19.5 keV. Utilizing the similar method, we obtained 25 nm in the horizontal direction and 40 nm in the vertical direction at 19.5 keV (note the vMLL used at this energy is different). The result is not shown here. Lastly, we found that the overall stability of the MLL-based microscope was excellent, with no observable degradation of focusing performance over 72 hours after the optics were aligned.

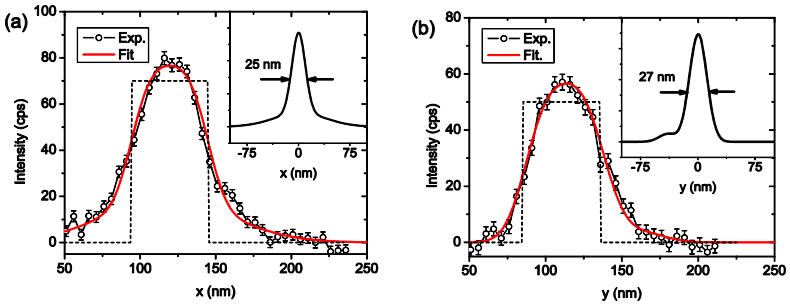

Fig. 6. A line scan across an isolated 50-nm line in *x* (a) and *y* (b) directions and their fits assuming a square function for the line (dashed). The insets show the fitted focus profiles. The experimental data is an average of 30 repeated scans with the background subtracted.

The nanofocusing capability that we experimentally demonstrated has immediate applications to many scientific areas. For example, imaging at the nanometer scale of spatial heterogeneities in real catalysts is essential to understand the diffusion of reactants and reaction products within the porous catalyst crystals or grains of sub-micrometer dimensions [21]. Nanoscale x-ray probe provides an ideal tool for nondestructive, label-free chemical imaging of catalytic solids. In biology, imaging trace metal in cells via x-ray fluorescence is of great interest [22]. Furthermore, broad classes of energy materials are based on thin films, where spatial inhomogeneities and local strain may play an important role in the properties of these materials.

4. Conclusion

In conclusion, we have demonstrated focusing of hard x-rays to a 2D focus of 25 nm horizontal × 27 nm vertical FWHM at a photon energy of 12 keV, and of 25 nm horizontal × 40 nm vertical FWHM at a photon energy of 19.5 keV. We achieved a 2D focusing efficiency of 17% at 19.5 keV. We have demonstrated x-ray fluorescence microscopy of test patterns with MLL nanofocusing optics. Nanometer imaging resolution with hard x-rays has been identified as a key objective for making full use of global investments in major x-ray source facilities. With the continuing development of MLL optics [23] and related nanopositioning capabilities, focusing x-rays with high efficiency to the nanometer scale is coming within reach.

Acknowledgments

We thank R. Winarski and P. Fuesz for their support in preparing the experiments. We thank R. Porter for implementation of instrument controls, and X. Jiao and A. Miceli for help with beamline controls. Work at Argonne, including use of the Advanced Photon Source and

#145575 - $15.00 USD Received 7 Apr 2011; revised 19 May 2011; accepted 22 May 2011; published 21 Jul 2011

Center for Nanoscale Materials, was supported by the Department of Energy, Office of Basic Energy Sciences under contract DE-AC-02-06CH11357. Work at Brookhaven was supported by the Department of Energy, Office of Basic Energy Sciences under contract DE-AC-02-98CH10886. One of the authors (H. C. Kang) would like to acknowledge the support by Basic Science Research Program through the National Research Foundation of Korea (NRF) funded by the Ministry of Education, Science and Technology (MEST No. R15-2008-006-01000-0).

#145575 - $15.00 USD Received 7 Apr 2011; revised 19 May 2011; accepted 22 May 2011; published 21 Jul 2011